Topographic mapping from digital aerial photogrammetry: a case study

Hassan G. El Ghazouly

Transportation Dept., Faculty of Eng., Alexandria University, Alexandria , Egypt

This study gives a brief overview of data acquisition method using photogrammetric technique and digital photogrammertic systems for topographic mapping. The suitability, the theoretical aspects, the procedure and the error influencing the data acquisition process of digital photogrammetric systems are discussed with the emphasis on the accuracy assessments of the collected data for topographic mapping. Special regard is given to the expected accuracy in using digital aerial photogrammetry, and levels of efficiency that will be achieved in deriving contour lines from extracted Digital Elevation Models (DEMs). The SURFER (Surface Mapping Software) is used for contour lines derivation and aids for the analysis of the results. Correlation coefficients of collected and extracted data relative to DEMs derived from the available contour lines have been calculated in addition to the systematic errors. Derived contour lines were superimposed on available contour lines for comparing the general agreement and the representation of local features.

يهتم هذا البحث بكيفية استخدام المساحة التصويرية الرقمية لاستنباط المعلومات الهندسية والدرجات الرمادية أو اللونية والمعلومات الوصفية الخاصة بمعالم سطح الأرض من الصور الرقمية الخاصة بها. وقد تم فى هذا البحث استخدام المواسح الرقمية في إدخال البيانات كما تم استخدام نظامين خاصين بإنتاج الخرائط الأول Wild Avioylyt BC2 والثانى DPW700 digital stereo ploter. وقد تم في هذا البحث دراسة الأخطاء المؤثرة على البيانات المأخوذة من المساحة التصويرية الرقمية على منطقة من شبه جزيرة سيناء مع التأكيد على متطلبات الدقة لإنتاج الخرائط الطبوغرافية. وقد وجد في هذا البحث أن أجهزة المساحة التصويرية الرقمية تعطى دقة أكبر من المساحة التصويرية الجوية التحليلية كما أوضح البحث أن إنتاج الخرائط الكنتورية من الصور الرقمية المصححة DEMs والمأخوذة بواسطة أسلوب مطابقة الصور باستخدام الأجهزة الرقمية تقلل من الزمن اللازم لتحويل الخرائط.

Keywords: Aerial photogrammety, Topographic map, Digital photogrammetory, DEMs.

1. Introduction

Topographic maps are of fundamental importance for econmic development and resource management in any country. The shortage in producing and updating topographic maps, especially in developing countries, can not be overcome by traditional surveying methods or aerial photogrammetry.

Aerial photogrammetric systems are concerned with transforming centrally projected overlapping photographis into three dimensional models at known scale representing the surface of the earth. These models are used for the extraction of geometric features and most of semantic features on the surface of the earth. On stereoplotters, three dimensional models (stereomodels) are formed through procedure of orientation.

In digital photogrammetrey there is a number of techaical advantages over analytical photogrammetry. Moreover, substantial subtasks can be automated. Automation can take the form of completely automatic batch processes or semi-automatic interactive processes. Batch processes are possible for point transfer, interior and relative orientation, DEM data generation, and geometric image transformation (orthoimage computation, generation of epipolar images and perspective views,... etc).In the latter process, a set of projective equations is applied to every pixel. For the other processes, image matching algorithms play the essential role in obtaining a solution [1].

2. Digital photogrammetry procedure

Digital photogrammetry has changed the process of mapping. Since digital photogrammetry deals only with digital images, then the scanning task must be added to the procedure. In the following sections, the different tasks of digital procedure will be discussed.

2.1. Scanning

The first task in digital photogrammetry procedure is the scanning of the diapositives as one of the most important tasks in the entire procedure. The idea is to completely capture the true radiometric quality of the aerial film while at the same time maintaining its geometry. The scanning task output is a raster data.

1- Raster data: could be a scanned aerial photograph. The display of the computer screen will simply be a duplicate of the photograph. The sharpness or resolution of the screen display is a function not only of the screen resolution but also of the geometric resolution of the scanner.

Raster data comes from scanning existing hardcopy documents, maps, or photographs. It is a rectangular equally spaced matrix or grid of pixels. Each cell or pixel within the matrix has a row and column address and a value associated with it, this value may relate to the intensity of a particular wavelength of the electromagnetic spectrum measured by a high altitude satellite, or be as simple as the colour reflected from ink on a scanned document. Scanning hardware measures the intensity of light reflected from or transferred through the scanned map, document, or photograph. The measured value can be 1,4 or 8 bits number and it is known as the depth of pixel.

2- Photogrammetric scanners: In all photographic scanners, light transmitted through or reflected from an illuminated photograph is projected onto a photosensitive surface which produces an electrical signal proportional to the variations in light intensity reaching that surface. The electric signal is then converted into a digital number by an electronic circuit for use as computer input[2].

There are several photodetectors used to convert pictorial information into digital form. The most commonly used photodetectors are the photo- multiplier and the Charge-Coupled Detectors (CCD) in line or matrix form.

Aerial photographs should be scanned with special scanners which have special specifications. What follows are the most important specifications:

- Geometric accuracy.
- Geometric resolution.
- Radiometric resolution.

2.2. Image matching

Two algorithms for image matching are available; area-based matching which is the preferred algorithm in photogrammetry and feature-based matching which is preferred in computer vision.

2.2.1. Area-based matching

Several techniques exist to measure the similarity. Probably the most popular of them is the correlation technique. The similarity between the gray level distribution in the target area and each subsearch area is simply expressed by the gray level difference D[3].

$$D = \sum_{i=1}^{n} \sum_{j=1}^{n} \left(g'_{ij} - g''_{ij} \right)^2 . \qquad (1)$$

In which g` represents gray levels of target area pixels. g`` represents gray levels of subsearch area pixels, and i and j are row and column locations respectively within the two areas.

Another popular technique for area based matching is the least squares area based matching in which the gray levels of the target and subsearch areas are considered as observations. Consequently, the following generic observation equation is formed [4].

$$R = g_t (X_t, y_t) - T^r [g_s T^g (x_s, y_s)].$$

Where, r is the residual vector of dimension n, $g_t (x_t, y_t)$ is the gray levels of the target area and, $g_s (x_s , y_s)$ are the gray levels of the subsearch area.

The gray levels $g_s(x_s, y_s)$ are modified by a radiometeric transformation T^r and a geometric transformation T^g.

2.2.2. Feature – based matching

There are two different approaches to feature based matching; points and edges.

In points approach, interest points are detected. The meaning of interest point is a mathematical definition based on gray value gradients. Interest operators are used to select a set of well scattered points in the left image such that each point contains sufficient information to produce a reliable match for corresponding points on the overlapping image.

There are different interest operators; e.g the Forstner interest operator detects points, corners, and centers of cercular features.Each pixel within a window of say, 5 x 5 pixels is regarded an edge element with an orientation derived from the gradient of the gray levels[4] as:

$$\nabla^T g(x, y) = [g_x(X, Y), g_y(X, Y)] . \quad (3)$$

For example, a corner can be detected at location X_o, Y_o by intersecting all edge elements. Likewise, the center of a circular feature is obtained by intersecting the normal of the edge elements.

Edges are the predominant features used in feature-based matching. Edges in the image refer to discontinuities in the gray levels. Numerous edge operators have been proposed. It may be classified into two types: first derivative and second derivative operators. First derive operators detect edges as the local maxima of the first derivative, which is approximated by the gradient of the gray values. Second derivative operators detect edges as the zero crossings of the second derivative which is most commonly approximated by the Laplacian of the gray levels [4].

Because edge operators enhance noise, it is important to smooth the images prior to edge detection. The Laplacian of the Gaussian, LoG, operator combines smoothing, with a Gaussian, with the second derivative. The definition is given (Ibid) as follows:

$$\nabla^2 G(x,y) = [\frac{x^2+y^2}{\sigma^2} - 2] e^{-\frac{x^2+y^2}{2\sigma^2}} . \quad (4)$$

Where, $\nabla^2 G(x,y)$ $\nabla$is the Laplacian of the Gaussian (LoG) and the size (ω) of the LoG operator refers to width of the central lobe and is related to the parameter σ of the Gaussian by:

$$\omega = 2\sqrt{2\sigma} , \quad (5)$$

The smoothing operation has a negative effect in that edges are dislocalized . In general, edge matching does not render the same high accuracy as area-based matching.

Generally, image matching is subject to blunders, especially in areas of low or repetitive texture. Additional problem scan occur in large scale imagery due to occlusions, height discontinuities in bult-up areas or forests.

2.3. Aerotriangulation using digital stereoplotters

Usually, point selection, point transfer, point measurement and final block adjustment have to be performed sequentially using point mark/transfer instruments and analytical plotters. Digital aero- triangulation can combine these steps into one integral procedure, and thus opens new possibilities for the overall performance. One key techniques is the application of matching procedures to digitized images, enabling a substantial automation of arial triangulation.

Digital methods offer several advantages in aero triangulation as compared to traditional methods[5]. Some of these advantages are:

- Image matching improves the accuracy of point transfer and thus the accuracy of the block as a whole.
- The image remains stable after scanning and the fast systematic scanning process minimizes the effects of film deformation, caused by heat dissipation of the measuring instrument.
- All the orientation parameters computed in block adjustment can be stored permanently for later use in subsequent phases like

interactive mapping or production of orthophotos.

2.4. Orientation using digital stereoplotter

The three well known phases of orientation are carried out as follows

- Interior Orientation: The purpose of interior orientation is to establish coordinate transformation between the pixel coordinate system of the digital image and the refined image coordinate system.

Practically in some systems, the software can find the center of the fiducial mark automatically and in others, the software can measure the fiducial marks automatically on images after the first one in the strip whose fiducial marks should be measured interactively.

- Relative Orientation: Relative orientation establishes the relative location of the two images.The relative orientation subtask is especially suited for automation, because a very small number of parameters, namely 5, need to be computed and a large amount of input data is available.

- Absolute orientation: The asbsolute orientation mainly depends on the identification and measurement of control points in the images which requires sufficient knowledge about these points. Its automation is rather difficult.

2.5. Resampling of digital images to epipolar geometry

To view overlapping pairs of digital images stereoscopically, the parallax direction of the images must be parallel to the eyebase of the observer, in other words, corresponding epipolar lines of the stereo pair must lie along corresponding rows of the digital images.

Digital images registered in epipolar geometry with respect to the object space are called normalized images. Thus exterior orientation elements, after absolute orientation, are to be used for transforming the original images to normalized images.

Either one of two transformations may be used to transform from original image to normalized image; transformation using collinearity condition or projective transformation.

- Transformation using collinearity: The collinearity condition equations can be used for the transformation of the original to normalized images. The transformation is represented in the following equations.

$$X_N = -f_N \frac{r_{11} x_o + r_{12}\ y_o - r_{13}\ f_o}{r_{13}\, x_o + r_{32}\, y_o - r_{33}\, f_o}, \qquad (6\text{-a})$$

$$Y_N = -f_N \frac{r_{21} x_o + r_{22}\ y_o - r_{23}\ f_o}{r_{31}\, x_o + r_{32}\, y_o - r_{33}\, f_o}. \qquad (6\text{-b})$$

Where, $r_{11}..., r_{33}$ are the elements of the normalized orthogonal rotation matrix R_N transforms the original images to the normalized images; f_o and f_N are the focal lengths of the original image and normalized image respectively, and x_o, y_o and X_N, Y_N are the photo coordinates of the original image and the normalized images, respectively.

The normalized rotation matrix R_N is a multiplication of two rotation matrices; the rotation from original images to true vertical images and the rotation from true vertical images to normalized images,

$$\mathbf{R_N = R_B\, R^T}. \qquad (7)$$

Where, $\mathbf{R^T}$ is the transpose matrix of exterior orientation elements which transforms the original images to true vertical images. R_N is an orthogonal matrix which transforms the object (ground) space to original image space, and R_B is the base matrix which is a resultant matrix which transforms the true vertical images to normalized images and its elements can be computed from the exterior orientation elements.

- Projective transformation: The projective transformation can be applied since both original images and normalized images are planar.

The projective transformation is represented in the following equation:

$$x_N = \frac{a_{11} x_o + a_{12} y_o + a_{13}}{a_{31} x_o + a_{32} y_o + 1}, \qquad (8\text{-a})$$

$$Y_N = \frac{a_{21}\, x_o + a_{22}\, y_o + a_{23}}{a_{31}\, x_o + a_{32}\, y_o + 1}. \qquad (8\text{-b})$$

where, a_{11} ... a_{32} are the projective unknown parameters,

3. DEM data acquisition

In digital photogrammetric systems, techniques of image matching are used to acquire DEM data automatically from digital stereopairs of aerial photograrhs. Compilation rates over two hundred points per second can be achieved on modern computers. The data produced have to be edited, however, and this can be very tedious and time consuming process[6].

3.1. Analysis of DEMs

The SURFER, version 5.00 surface mapping software by Golden Software, incorporation is used in this study to generate three grid DEMs from the ASCII file, 50m, 25 and 10m grid spacing and they are corrected for systematic errors due to the interpolation mathematical model.

First the observations are checked for the presence of systematic error.

A systematic error can be present in the observations [7] if,

$$[d]^2 \geq [dd]. \qquad (9)$$

Where, [ ] indicates the summation of similar terms instead of the common sigma Σ, and [d] is the summation of differences (z_2-z_1) between the pairs of elevations observations.

When this condition is achieved, the systematic part of error (d_s) present in the observations is calculated from the following formula [7].

$$d_s = \frac{[d]}{n}, \qquad (10)$$

where; n is the number of grid points.

In the case of presence of systematic errors, the residuals v_i must be used in the calculations of the Root Mean Square Errors (RMSEs) instead of the differences d_i, because the differences in this case are not pure random variables. The residuals can be calculated from the following formulas,

$$v_i = d_s - d_i,$$

or

$$[vv] = [dd] - \frac{[d]^2}{n}. \qquad (11)$$

The RMSE of elevation differences is calculated from the following equation,

$$\text{RMSE} = \pm \sqrt{\frac{[vv]}{(n-1)}}. \qquad (12)$$

The RMSE of the systematic part of error is calculated from the following equation,

$$\text{RMSE ds} = \pm \sqrt{\frac{[vv]}{n(n-1)}}. \qquad (13)$$

The correlation coefficients (ρ) between the elevations of DEMs collected by the Aviolyt BC2 or extracted by the DPW770 which will discussed latter. and those derived from the available contour lines of the analogue AG1 stereoplotter are computed using the following formula [7],

$$\rho_{z_1,z_2} = \frac{\text{cov}(z_1, z_2)}{RMSE_1\ RMSE_2}. \qquad (14)$$

Where, $RMSE_1$ and $RMSE_2$ are the RMSEs of z_1 and z_2 respectively and are calculated from eq. (15), and cov (z_1, z_2) is the covariance of z_1 and z_2 and it is calculated using eq. (16)

$$\text{RMSE} = \pm \sqrt{\frac{[z_{1i} - \bar{z}]^2}{(n-1)}}. \qquad (15)$$

Where, z is the mean.

$$\text{cov}\,(z_1,z_2) = \pm \frac{n[z_1 z_2] - [z_1][z_2]}{n(n-1)}. \qquad (16)$$

4. Applications and results

The area of sinai panensula east Yalaq mountain 90km south El – Arish city fig. 1 is choosen for the application of this paper [8].

The area was covered by aerial photography at a flying height 4020m as shown in fig. 2-a and 2-b.

The Camera calibrated focal length was 153.21 mm. The fiducial marks coordinates with origin at point of symmetry are listed in table 1.

Table 1
Fiducial marks coordinates (μm)(origin is the point of symmetry)

Fiducial No.	X	Y
1	105999	-106001
2	-105997	-105998
3	-105998	106000
4	105997	105999

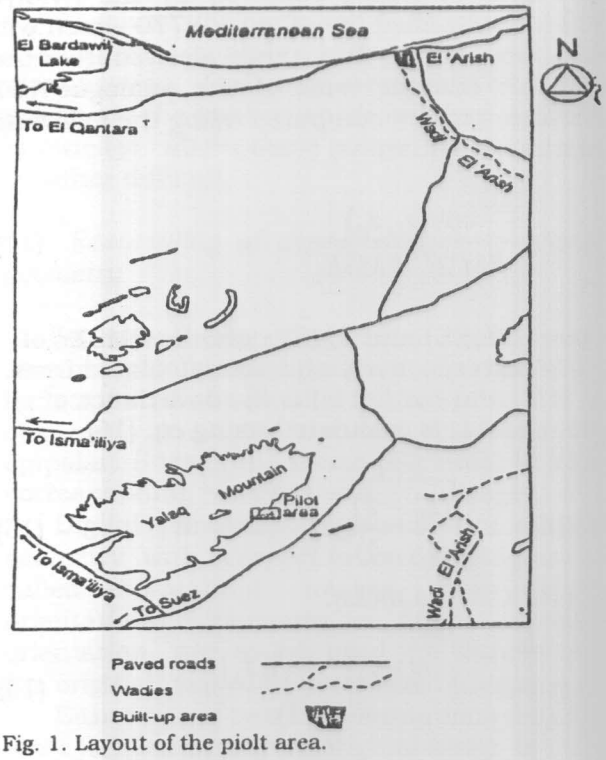

Fig. 1. Layout of the piolt area.

The radial lens distortion values are listed in table 2. and table 3. contains the ground coordinates of five phote control point.

Fig. 3. represents the contour lines for the area of investigation digitally compiled using AG1 analogue stereoplotter.

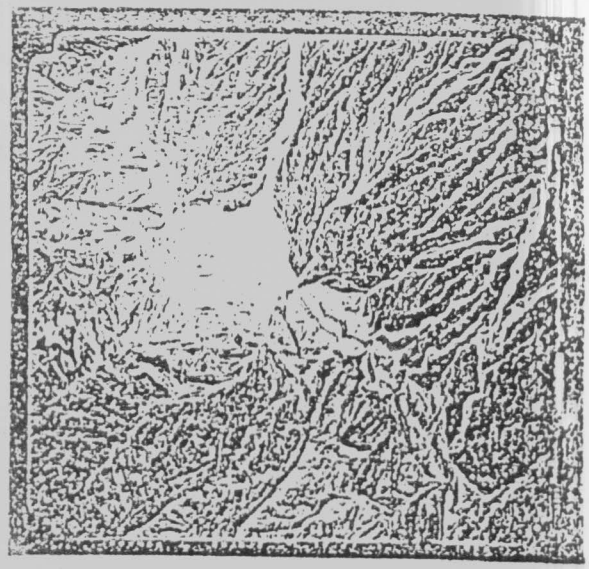

Fig. 2-a. Left photo of the stereopair.

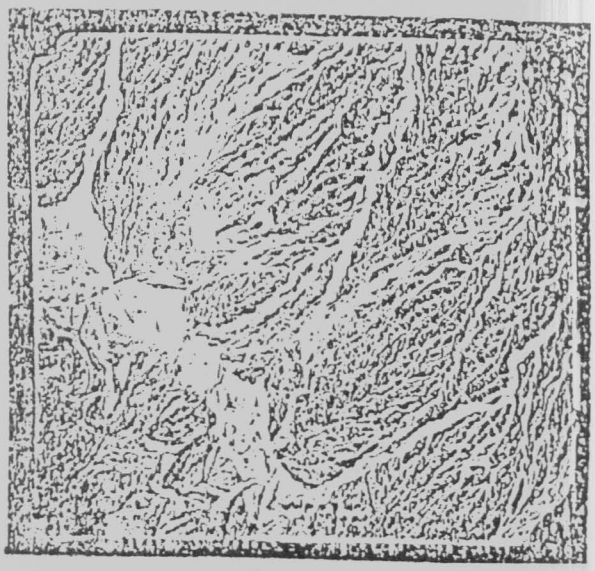

Fig. 2-b. Right photo of the stereopair.

Table 2
Radial lens distortion values in (μm) (origin is the point of symmetry, and interval equal 10mm)

r(mm)	10	20	30	40	50	60	70	80	90	100	110	120	130	140	150
d(μm)	0.1	0.0	-0.4	-0.3	-0.7	-0.8	-0.8	-0.8	-0.1	0.1	0.3	-0.1	0.0	0.3	1.8

Table 3
Ground coordinates of the five photo control points

Point No.	X (m)	Y (m)	Z (m)
221	9285.66	6653.97	404.743
222	6969.66	6359.04	435.099
223	4808.97	6159.28	472.381
231	9130.86	8522.54	422.293
233	4917.57	7965.08	709.604

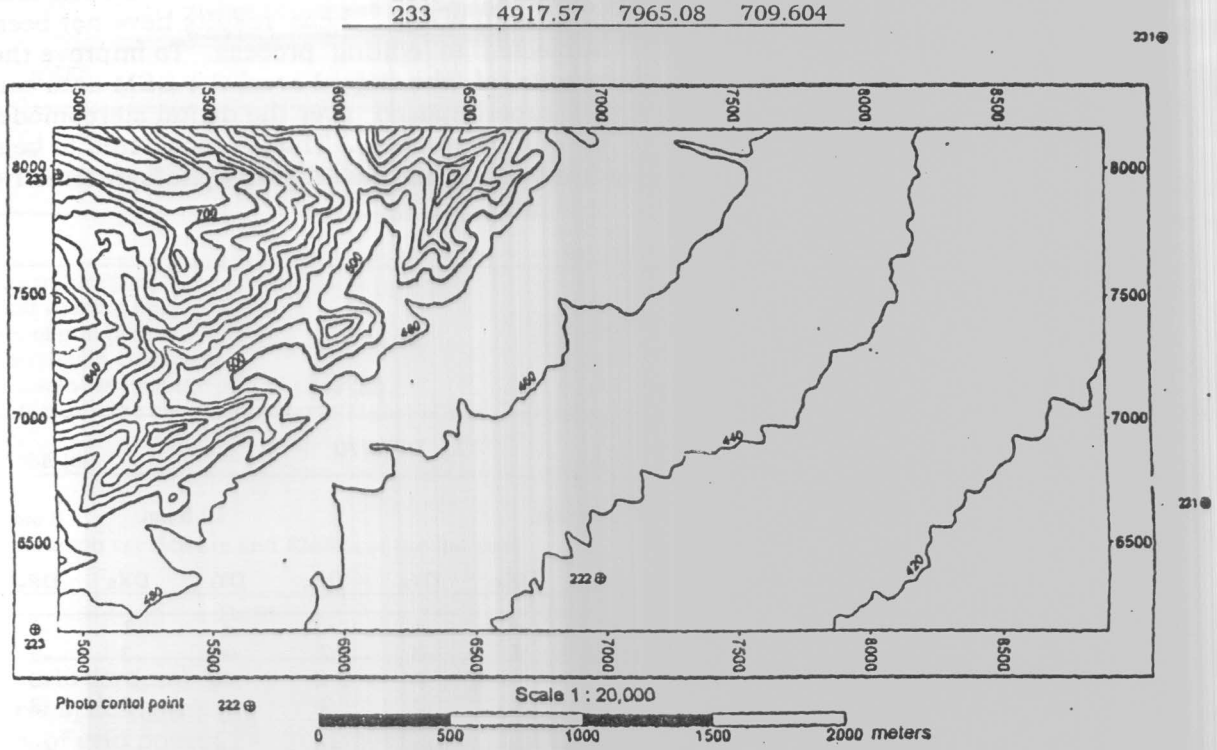

Fig.3. Available contour lines digitally compiled using AG1.

4.1. Analytical comparison

In this study two photogrametric systems were used. The first is Upgraded Wild Aviolyt BC2 by Leica analytical photogrametric system. The second is Leica/Helava digital photgramaetric system of Techno Scient (DSW 200 photogramonetric Scanner and DPW 770 digital Stereoplotter).

Four fiducial marks have been measured on the digital images before scanning and an affine transformation model is used to relate pixel coordinate to the corresponding given fiducials coordinates, the results of transformation are listed in table 4.

Residuals and RMSEs are given in table 4 from the least squares adjustmests for each photogroph and each image, using 25μm resolution in the Aviolyt BC2 and using 12.5μm as well as 25 μm in the DPW770.

The RMSE ranges from ± 2 μm to ± 4 μm for the DPW770 and from ± 1 μm to ± 6 μm for the Aviolyt BC2.

Table 5. shows the residuals in photo and pixel coordinates and their RMSE of the five photo control points. The RMSE values of the

25 μm resolution in the DPW770 ranges from ± 0.75 to ± 2.5 μm, and those of the Aviolyt BC2 vary from ± 0.24 to ± 3.19 μm but for 12.5 μm range from ± 0.39 to ± 2.13 μm.

Table 6. shows the residuals in ground coordinate of the five photo control points. The RMSE values of 25μm resolution in the DPW770 vary from ± 0.255 to ± 0.376 m and in case of the Aviolyt BC2 range from ± 0.094 to ± 0.486m. But in case of DPW770 with 12.5 μm resolution it gives a range from ± 0.051 to ± 0.168m which is relatively better than that results from the 25 μ m.

DX_G, DY_G, and DZ_G are the residuals in ground coordinates of the five photo control points.

Table 7. lists the correlation of coefficients and RMSEs values computed for the pilot area as a whole. Generally, the Aviolyt BC2 gives more accurate results than the DPW 770.

In the flat part of the pilot area, the correlation coefficients of the DEM collected by the Aviolyt BC2 and those of the DEMs extracted by the DPW 770 are nearly identical. Table 8 displays the values of the correlation coefficients and RMSEs of the flat part of the area.

Table 9. list the values of the correlation coefficients and RMSEs of the rugged part of the pilot area. From table 9. the DEM collected by the Aviolyt BC2 is more accurate than that of the DPW770. These results have not been subjected to editing process. To improve the results of the rugged area, the DEM data can be superimposed over the digital stereomodel to edit it manully. This is cosidered to be a drawback of the digital photogrammetric systems [7].

Table 4
Residuals in fiducial marks coordinates (μm)

Fiducial No.	Aviolyt BC2				DPW770							
					25μm				12.5 μm			
	DX_L	DY_L	DX_R	DY_R	DX_L	DY_L	DX_R	DY_R	DX_L	DY_L	DX_R	DR_R
1	1	-1	2	-6	-2	2	-4	3	-2	4	3	-3
2	-1	2	-2	6	2	-2	4	-3	2	-4	-3	-3
3	1	-2	3	-6	-2	2	-4	3	-2	4	3	-3
4	-1	1	-3	6	2	-2	4	-3	2	-4	-3	-3
RMSE	±1	±1.6	±2.6	±6	±2	±2	±4	±3	±2	±4	±3	±3

DX_L DY_L are the residuals in fiducial marks coordinates for the left photo and DX_R, DY_R are the residuals in fiducial marks coordinates for the right photo.

Table 5
Residuals in photo coordinates and pixel coordinates (μm)

Point No.	Aviolyt BC2 Photo coordinates				DPW770 Pixel coordinates							
					25μm				12.5 μm			
	DX_L	DY_L	DX_R	DY_R	DX_L	DY_L	DX_R	DY_R	DX_L	DY_L	DX_R	DR_R
221	0.10	2.40	0.10	-2.20	1.00	-2.50	0.75	1.00	0.13	0.25	-0.39	0.25
222	-0.30	-4.80	0.40	4.80	-2.00	2.50	0.75	-1.00	0.00	-0.63	-0.25	1.00
223	0.40	2.50	-0.30	-2.90	1.75	-3.50	-1.50	2.25	-2.13	-0.25	2.63	0.50
231	-0.10	-2.40	0.00	2.60	-1.50	0.75	-0.25	-0.50	-0.63	1.00	1.38	-1.23
233	-0.30	-2.90	0.20	2.80	0.75	2.50	0.25	-1.50	1.00	0.13	-1.75	-0.63
RMSE	±0.27	±3.14	±0.24	±3.19	±1.50	±2.50	±0.75	±1.25	±2.13	±0.39	±1.75	±0.50

Table 6
Residuals in ground coordinates (m)

Point No.	Aviolyt BC2			DPW770					
				25μm			12.5 μm		
	DX_G	DY_G	DZ_G	DX_G	DY_G	DZ_G	DX_G	DY_G	DZ_G
221	0.126	-0.108	0.299	0.500	-0.322	0.149	-0.084	-0.005	-0.19
222	0.387	0.053	0.131	-0.375	0.365	0.144	-0.087	0.121	0.089
223	-0.680	0.002	-0.410	0.095	-0.409	-0.326	0.171	0.087	-0.054
231	-0.260	0.094	-0.606	-0.487	0.028	-0.203	0.220	-0.036	-0.038
233	0.697	-0.143	-0.006	0.267	0.338	0.226	-0.220	-0.168	0.021
RMSE	±0.486	±0.094	±0.358	±0.376	±0.322	±0.225	±0.168	±0.102	±0.051

Table 7
Correlation coefficients and RMSEs of the DEM results of the pilot area

Item	Aviolyt BC2	DPW770			
Resolution (μm)	--	25		12.5	
Grid spacing (m)	50	50	25	50	25
No. of grid points	3321	3321	13041	3321	13041
Correlation coefficient	0.999	0.991	0.996	0.989	0.996
Constant systematic part of error (m)	+0.96	-1.93	-1.18	-3.54	-1.17
RMSE of the constant systematic part of error (m)	±0.06	±0.18	±0.06	±0.21	±0.06
RMSE (m)	±3.54	±10.12	±6.56	±11.87	±6.50

Table 8
Correlation coefficients and RMSEs of the flat part

Item	Aviolyt BC2	DPW770			
Resolution(μm)	--	25		12.5	
Grid spacing(m)	50	50	25	50	25
No. of grid points	2341	2341	9265	2341	9265
Correlation coefficient	0.986	0.987	0.988	0.986	0.987
Constant systematic part of error(m)	+0.28	-1.26	-0.96	-1.34	-0.76
RMSE of the constant systematic part of error(m)	±0.07	±0.06	±0.03	±0.07	±0.03
RMSE(m)	±3.18	±3.12	±2.96	±3.19	±3.04

Table 9
Correlation coefficients and RMSEs values of the rugged part

Item	Aviolyt BC2	DPW770					
Resolution(μm)	--	25			12.5		
Grid spacing(m)	50	50	25	10	50	25	10
No. of grid points	980	980	3776	23017	980	3776	23017
Correlation coefficient	0.999	0.977	0.991	0.998	0.970	0.991	0.997
Constant systematic part of error(m)	+2.57	-3.52	-1.72	+0.81	-8.80	-2.20	-0.20
RMSE of the constant systematic part of error(m)	±0.12	±0.57	±0.18	±0.04	±0.65	±0.18	±0.05
RMSE(m)	±3.83	±17.90	±11.25	±5.55	±20.35	±11.35	±5.89

4.2. Contouring from DEMs

The SURFER software has been used to derive contour lines with 20 m intervals from the ASCII files of the DEM collected by the Aviolyt BC2 and the DEMS estracted by the DPW770 for the 25 μm resolution only since the 12.5 μm resolution does not yield an improvement in the DEMs accuracy. Fig.3 shows the derived contour lines from DEM collected by the Aviolyt BC2. Fig. 4 to 7 show the derived contour lines from the three DEMs extracted by the DPW770. The quality of a contour map is especially judged by the fidelity with which small details and fine morphological features are represented in the contour lines. There are no clear objective criteria with which to describe or measure the fidelity of contour lines [9].

4.3. Surface visualization

Terrain surface plots are generated using the SURFER software. Surface plots are 3D representations of the grid file that can be displayed with any combination of X and Y profiles. The 3D views of the terrain surface generated from the three 25m, 50m and 10m grid spacing are also examined.

The quality of a terrain surface plot is especially judged by the fidelity with which different hills are represeted in the 3D view of the surface.

5. Conclusions

From this study the digital stereoplotter provides more accurate interior and exterior orientation than that obtained by the analytical stereo plotter.

In flat areas with good texture, the digital stereoplotter gives more accurate results than that of the analytical stereoplotter. In rugged areas, DEM extracted with image matching by the stereoplotter contains errors. These errors are decreasing with the decreasing of the grid space and should be edited manually.

The digital system requires the use of smaller grid spacing than those used in the analytical system to get reliable results. Decreasing pixel size does not mecessarly lead to an inccrease in accuracy. Finally, deriving contour lines from DEMs extacted by image matching algorithms using digital stereoplotters reduces the time required for map compilation.

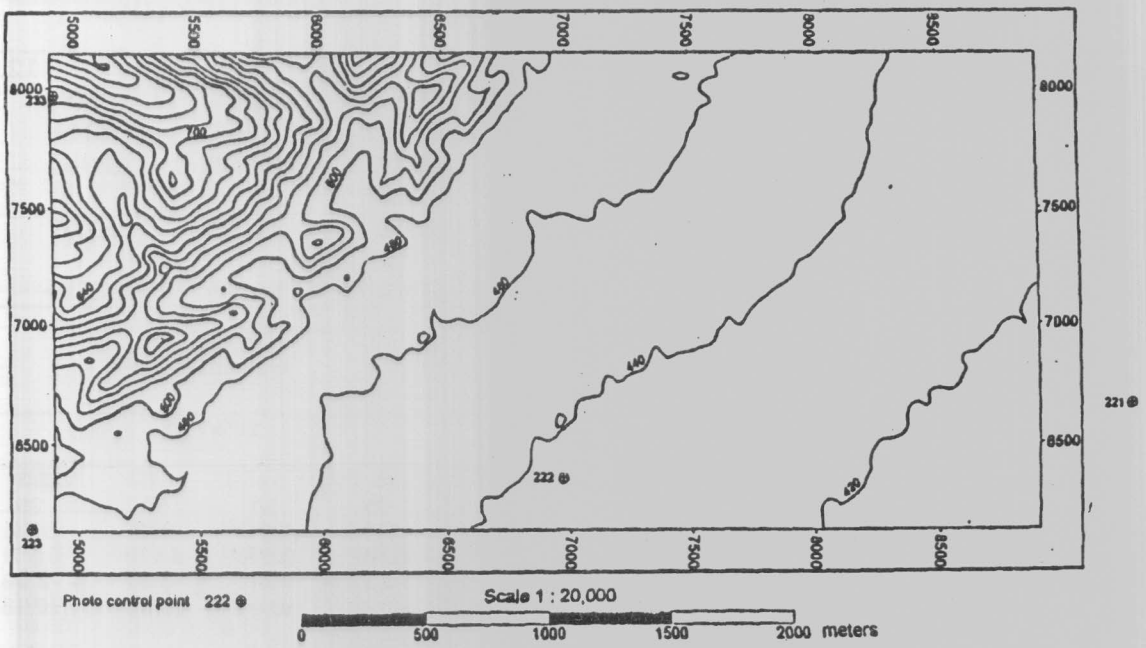

Fig. 4. Contour lines derived from 50 m grid spacing DEM collected by the Aviolyt BC2.

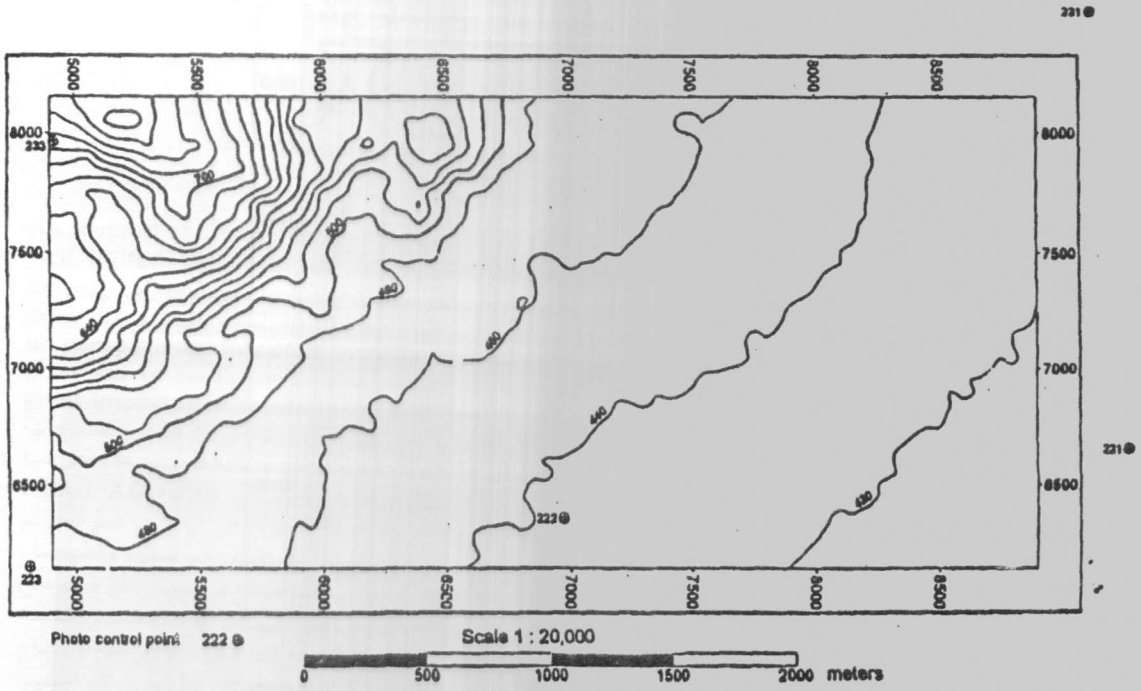

Fig. 5. Contour lines derived from the 50 m grid spacing DEM extacted by DPW770.

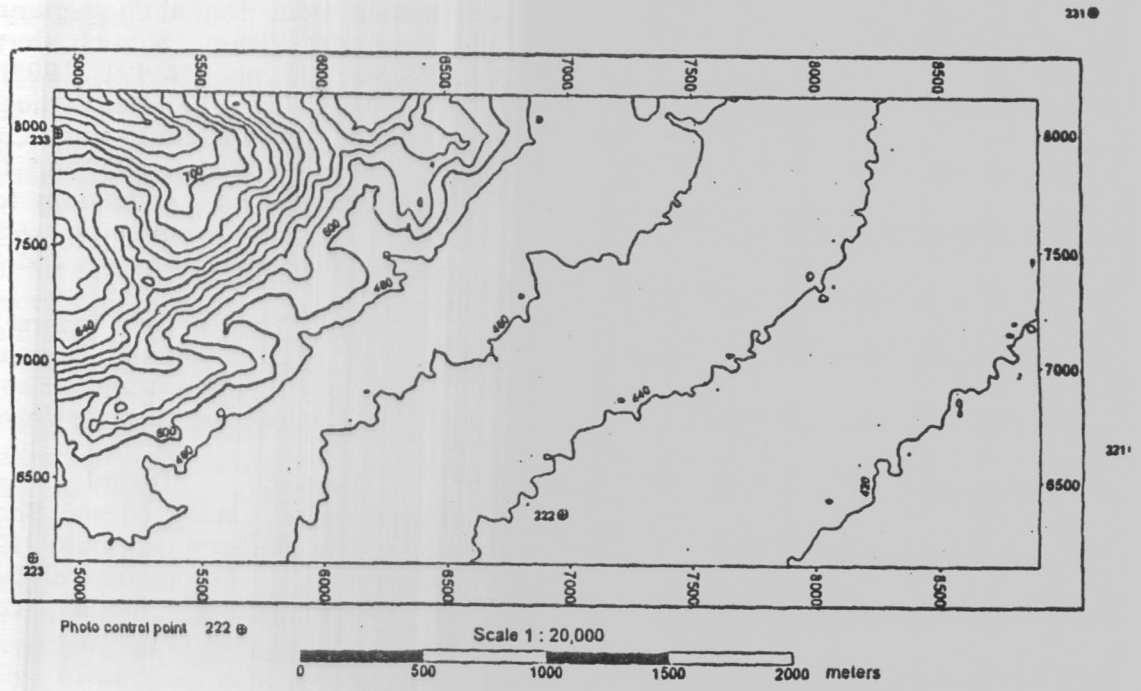

Fig. 6. Contour lines derived from the 25 grid spacing DEM exracted by DPW770.

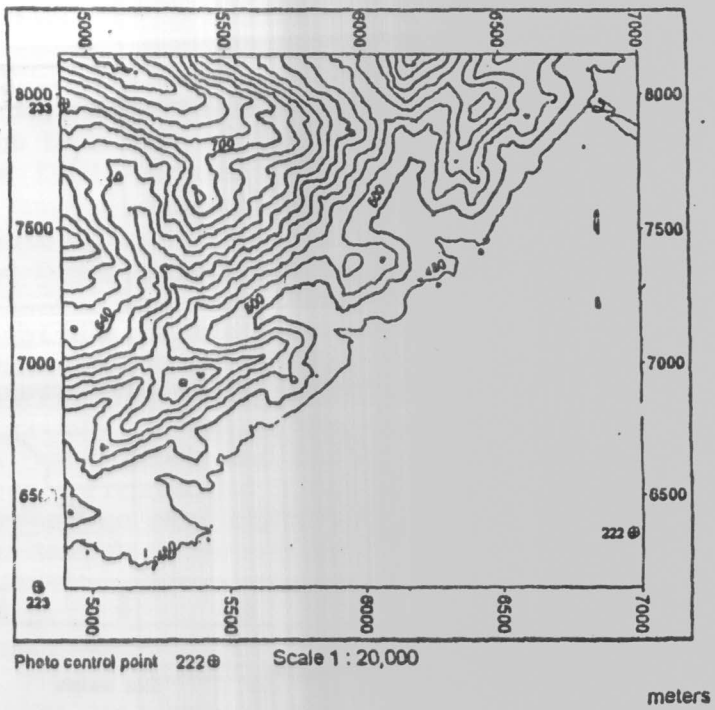

Fig. 7. Contour lines derived from the 10m grid spacing DEM extracted by DPW 770.

Refernces

[1] C. Heipke, "State - of - the - art of Digital Photogrammetric Workstations for Topographic Application", PE & RE, Vol. 61 (1), pp. 49 – 56 (1995).

[2] J.S. Montuori, " Image Scanner Technology", PE & RS, Vol.46 (1), pp. 46 – 61 (1980).

[3] P.R., Wolf, " Elements of Photogrammetry" Second Edition, Mc Graw- Hill Book Company (1986).

[4] T. Schenk, " Algorithms and Software Concepts for Digital Photogrammetric Work Stations: Research Activities in Digital Photogrammetry at Ohio State University, Schent, T. (ed.). Report No. 418, Department of Geodetic Science and Surveying, Ohio State University, pp. 17-36 (1992).

[5] J. Jaakkoia, and T. Sarjakoski, "OEEPE Research Project Aerotriangulation using Digitized Images Preliminary Results," ISPRS, commission III symposium, Spatial Information from Digital Photogrammetry and Computer Vision, Munich, Germany Vol. 30, part 3/1, pp. 416-421, (1994).

[6] F. R. Norvelle, "Using Iterative Orthophoto Refinements to Generate and Correct Digital Elevation Models (DEMs)," Digita Photogrammetry: An Addendum to the Manual of Photogrammetry, ASPRS, Bethesda, Maryland, USA, pp. 151 – 155 (1996).

[7] R.A. Ismail, "Theory of Errors and Adjustment of Observations", Department of Surveying Engineering, Shoubra, Faculty of Engineering, Zagazig University (1981).

[8] E.S. Ammar; "Digital Areal Photogrammetry", M.Sc. thesis, Shoubra Faculty of Eng., Zagazig University (1997).

[9] F. Ackermann, " Automation of Digital Aerial Triangulation," INPHO GmbH, Stuttgart, (1995).

Received June 25, 2001
Accepted Augusts 27, 2001